STRUCTURAL CONTROL AND HEALTH MONITORING
Struct. Control Health Monit. 2010; **17**:152–177
Published online 11 July 2008 in Wiley InterScience
(www.interscience.wiley.com). DOI: 10.1002/stc.281

Using component mode synthesis to estimate the restoring force of an isolation layer subjected to earthquakes

Liyu Xie*,† and Akira Mita

Department of System Design Engineering, Keio University, 3-14-1, Hiyoshi, Yokohama 223-8522, Japan

SUMMARY

A new method for estimating the restoring force of an isolation layer in a base-isolated system is proposed. The hybrid motion equation involving the modal coordinates and the physical coordinates is derived by component mode synthesis. This significantly reduces the number of unknown parameters after the mode shape information of the superstructure is substituted and makes it possible to identify the isolation layer directly and locally. The effectiveness of this method was validated in a simulation example and in an application to an actual base-isolated building. The difficulty lies in how to describe the state of a nonlinear device of a real structure. In this paper, the amplitude-dependent equivalent stiffness and damping coefficient are adopted to describe the nonlinearity of the isolation layer. The identified results by our proposed method reconfirm the experimental observation of nonlinearity in the layer made up of isolators.

KEY WORDS: component mode synthesis; mode expansion; hysteresis; amplitude dependent; identifiability

1. INTRODUCTION

Since the Kobe and Northbridge earthquake, base-isolation systems such as the friction pendulum and elastomeric-bearing systems have gradually come into use to alleviate the damage of structures. These systems isolate the superstructure from the ground, shift its natural frequency from the destructive range of ground motion, and enable it to absorb more energy without suffering damage. They have been shown to effectively protect structures from the effects of large earthquakes, but their effectiveness is largely determined by the behavior of the isolators that assimilate a large amount of the input seismic energy and reduces interstory drifts and floor accelerations. If the isolators degrade or fail, the structure will lose its ability to resist earthquakes. Therefore, it is important to assess the condition of isolators for monitoring the base-isolated structures.

*Correspondence to: Liyu Xie, Department of System Design Engineering, Keio University, 3-14-1, Hiyoshi, Yokohama 223-8522, Japan.
†E-mail: liyuxie@z3.keio.jp

Received 14 November 2007
Revised 12 April 2008
Accepted 15 May 2008

The damage detection reviewed by Doebling *et al.* [1] is accomplished by evaluating changes in dynamic properties such as the natural frequencies, mode shapes, and modal damping. This, however, is valid only in the linear domain. These properties cannot indicate the status of a nonlinear system because in a nonlinear system they will vary with the intensity of excitation even when the system is intact. Isolators exhibit nonlinear and hysteretic properties under experimental conditions [2], and the responses of four base-isolated buildings were investigated by Stewart *et al.* [3]. The stiffness and damping of the seismic isolation systems were isolated and evaluated; the systems were found to respond with a hysteretic action that strongly depended on the vibration amplitude. Because of the hysteresis, the stiffness of the isolators decreased significantly with increasing amplitude. Tobita [4] also evaluated the dynamic properties of actual buildings by modeling the structure as a linear, time-invariant system in each time segment. The variation in the damping and frequency with the input intensity was observed, and the distinctive amplitude-dependent damping characteristics of based-isolated structures were found.

A base-isolated system consists of two very different subsystems: the superstructure and the isolation layer. The isolation layer of a base-isolated structure is composed of rubber bearing isolators that typically have damping ratios up to 20%, while the superstructure is just an ordinary building with a very low damping ratio of its first mode. The conventional damage indices such as the modal frequencies and mode shapes are insensitive to local damage and thus cannot be used to quantify damage accurately. In addition, the nonlinearity of the system makes these indices invalid for damage detection. A direct and local identification method is therefore better than one using the conventional indices. This paper presents a new algorithm for estimating the restoring force of the isolation layer by component mode synthesis (CMS). In addition, the amplitude-dependent stiffness and damping coefficients, which are regressed from the restoring force of the isolation layer, are utilized to represent the nonlinear state of the layer.

2. ESTIMATING RESTORING FORCE BY COMPONENT MODE SYNTHESIS

CMS is a technique used to perform the dynamic analysis of structures by means of substructuring or decomposing the overall structure into several substructures whose boundary conditions are compatible in a specified way. This technique is quite useful for the dynamic analysis of complex structures in structural engineering, especially when the substructures have dynamic characteristics so different that the coupled structure has nonclassical vibration modes. In this paper, the state of the isolation layer is our concern and the number of the accelerometers mounted is limited. CMS is therefore used to derive the hybrid motion equation involving the modal parameters of the superstructure as well as the physical parameters of the isolation layer.

The CMS methods presented by Hurty [5] can be classified into four groups: fixed-interface methods, free-interface methods, hybrid-interface methods, and loaded-interface methods. These groups differ from each other mainly in the choice of the supplementary Ritz vectors, the associated generalized coordinates, and the coupling procedure. CMS methods have been reviewed by Craig [6] and others. In this paper, the fixed-interface method is adopted.

The base-isolated structure shown in Figure 1 consists of two substructures: a superstructure and a base-isolation layer. The superstructure is considered to be a linear system, and

DOI: 10.1002/stc

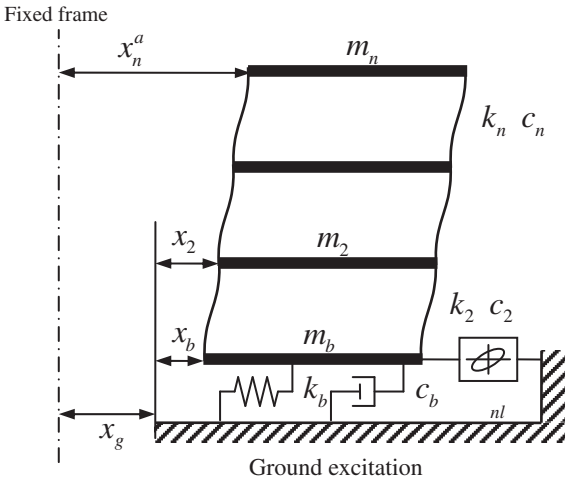

Figure 1. Structure model.

the base-isolation layer has both linear and nonlinear components. The linear component has a stiffness k_b and a damping coefficient c_b, and the nonlinear component has a restoring force of f_{nl}. There are many choices for the nonlinear model, but in the present case a hysteretic model is used because the rubber bearings of the isolation layer possess strong hysteresis. The model is described in detail in Section 7.

The dynamic equation of the overall structure is written as

$$\mathbf{M}\ddot{\mathbf{x}} + \mathbf{C}\dot{\mathbf{x}} + \mathbf{K}\mathbf{x} + \begin{Bmatrix} \mathbf{0} \\ f_{\mathrm{nl}} \end{Bmatrix} = -\mathbf{M}\mathbf{r}\ddot{x}_{\mathrm{g}} \tag{1}$$

$$\mathbf{F}_{\mathrm{nl}} = \begin{Bmatrix} \mathbf{0} \\ f_{\mathrm{nl}} \end{Bmatrix}$$

$$\mathbf{M} = \begin{bmatrix} m_n & & & 0 \\ & \ddots & & \\ & & m_2 & \\ 0 & & & m_b \end{bmatrix}$$

$$\mathbf{M}\mathbf{r} = [m_n \quad \cdots \quad m_2 \quad m_b]^{\mathrm{T}}$$

$$\mathbf{K} = \begin{bmatrix} k_n & -k_n & & & 0 \\ -k_n & k_n + k_{n+1} & -k_{n+1} & & \\ & & \vdots & & \\ & & -k_3 & k_3 + k_2 & -k_2 \\ 0 & & & -k_2 & k_2 + k_b \end{bmatrix}$$

DOI: 10.1002/stc

$$\mathbf{C} = \begin{bmatrix} c_n & -c_n & & & 0 \\ -c_n & c_n + c_{n+1} & -c_{n+1} & & \\ & & \vdots & & \\ & & -c_3 & c_3 + c_2 & -c_2 \\ 0 & & & -c_2 & c_2 + c_b \end{bmatrix}$$

where **K**, **C**, and **M** are, respectively, the stiffness, damping, and mass matrices; x is the displacement relative to the ground; and $\ddot{x}_{\mathrm{g}}$ is the ground acceleration.

Moving the nonlinear term to the right-hand side, we obtain

$$\mathbf{M}\ddot{\mathbf{x}} + \mathbf{C}\dot{\mathbf{x}} + \mathbf{K}\mathbf{x} = -\mathbf{M}\mathbf{r}\ddot{x}_{\mathrm{g}} - \mathbf{F}_{\mathrm{nl}}$$

The whole structure is separated into two substructures that have a common interface as shown in Figure 2. In addition, we impose a fixed boundary condition on this interface and make it unable to deform and move. These two substructures can therefore be treated as independent structures and can generate their own modal information. Our focus in this paper is not on how to retrieve the overall modal information by integrating substructures. Instead, we are trying to transform the traditional dynamic equations either in physical coordinates or modal coordinates into a hybrid form by CMS. The hybrid dynamic equations describe both the linear modal information of the superstructure and the nonlinear physical model of the isolation layer.

The equilibrium equation of the superstructure is

$$\mathbf{M}_s\ddot{\mathbf{x}}_s^{\mathrm{r}} + \mathbf{C}_s\dot{\mathbf{x}}_s^{\mathrm{r}} + \mathbf{K}_s\mathbf{x}_s^{\mathrm{r}} = -\mathbf{M}\mathbf{r}_s\ddot{x}_b^{\mathrm{a}} \tag{2}$$

where

$$x_b^{\mathrm{a}} = x_{\mathrm{g}} + x_b$$

and

$$\mathbf{x}_{\mathrm{s}}^{\mathrm{r}} = \mathbf{x}_{\mathrm{s}} - x_{\mathrm{b}}$$

The superscript r indicates coordinates relative to the fixed interface, while the superscript a indicates absolute coordinates. The subscripts s and b, respectively, denote the superstructure

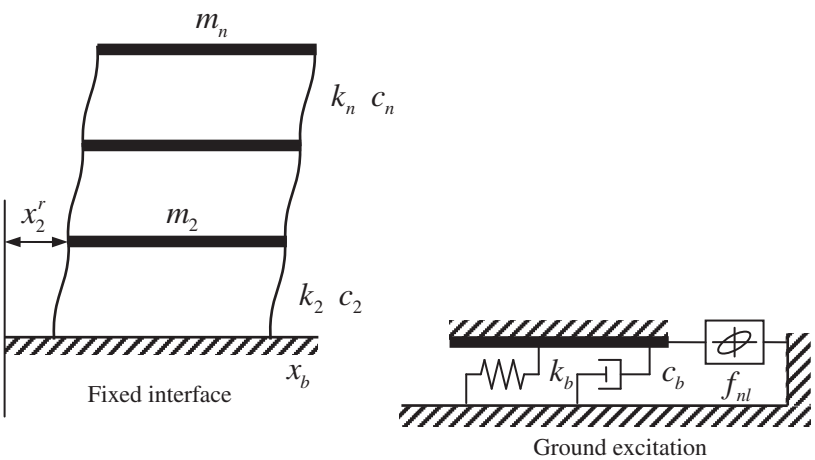

Figure 2. CMS: fixed-interface method.

DOI: 10.1002/stc

and the isolation layer. We assume that the damping matrix of the superstructure is proportional to the stiffness matrix. That is, $\mathbf{C}_s = \alpha \mathbf{K}_s$.

Rewriting the equation of superstructure in modal coordinates, we have

$$\boldsymbol{\Phi}_s^{\mathrm{T}} \mathbf{M}_s \boldsymbol{\Phi}_s \ddot{\boldsymbol{\xi}}_s + \boldsymbol{\Phi}_s^{\mathrm{T}} \mathbf{C}_s \boldsymbol{\Phi}_s \dot{\boldsymbol{\xi}}_s + \boldsymbol{\Phi}_s^{\mathrm{T}} \mathbf{K}_s \boldsymbol{\Phi}_s \boldsymbol{\xi}_s = -\boldsymbol{\Phi}_s^{\mathrm{T}} \mathbf{M} \mathbf{r}_s \ddot{x}_b^{\mathrm{a}} \tag{3}$$

where $\boldsymbol{\Phi}_s$ is the fixed-interface normal mode of the superstructure and $\boldsymbol{\xi}_s$ is the modal coordinate. $\mathbf{x}^{\mathrm{r}}$ is related to the modal coordinates as follows: $\mathbf{x}^{\mathrm{r}} = \boldsymbol{\Phi}_s \boldsymbol{\xi}_s$.

If $\boldsymbol{\Phi}_s$ is normalized in such a way that

$$\mathbf{M}_s^* = \boldsymbol{\Phi}_s^{\mathrm{T}} \mathbf{M}_s \boldsymbol{\Phi}_s = \mathbf{I}$$

We have the relations

$$\mathbf{K}_s^* = \boldsymbol{\Phi}_s^{\mathrm{T}} \mathbf{K}_s \boldsymbol{\Phi}_s = \boldsymbol{\omega}^2$$

and

$$\mathbf{C}_s^* = \boldsymbol{\Phi}_s^{\mathrm{T}} \mathbf{C}_s \boldsymbol{\Phi}_s = \alpha \boldsymbol{\omega}^2$$

Equation (3) can be expressed by

$$\mathbf{M}_s^* \ddot{\boldsymbol{\xi}}_s + \mathbf{C}_s^* \dot{\boldsymbol{\xi}}_s + \mathbf{K}_s^* \boldsymbol{\xi}_s = -\boldsymbol{\Phi}_s^{\mathrm{T}} \mathbf{M} \mathbf{r}_s \ddot{x}_b^{\mathrm{a}} \tag{4}$$

where $\boldsymbol{\omega}$ is the undamped frequency.

The physical displacements of the superstructure in local coordinates are expressed as a linear combination of its substructure modes. After some algebraic transformations, the displacements of the superstructure in general coordinates can be represented by a set of Ritz vectors:

$$\mathbf{x}_s = \mathbf{Q} \begin{Bmatrix} \boldsymbol{\xi}_s \\ x_b \end{Bmatrix}$$

where x_b is the displacement of the isolation layer representing the interface displacement. The boundary condition of its fixed interface determines the Ritz vectors [7] as

$$\mathbf{Q} = \begin{bmatrix} \boldsymbol{\Phi}_s & \boldsymbol{\Psi}_s \end{bmatrix}$$

where $\boldsymbol{\Psi}_s$ is the constraint mode associated with the fixed interface. It is the superstructure deformation obtained by imposing one unit displacement on the fixed interface. In this case the superstructure is constrained only by the base layer. Therefore, $\boldsymbol{\Psi}_s = \mathbf{1}$.

The overall physical coordinates can be transformed to the hybrid coordinate, which contains the modal coordinates of the superstructure $\boldsymbol{\xi}_s$ and the physical coordinate of the base isolator $\ddot{x}_b$:

$$\mathbf{x}_s = \boldsymbol{\Phi}_s \boldsymbol{\xi}_s + \boldsymbol{\Psi}_s x_b$$

$$\mathbf{x} = \begin{Bmatrix} \mathbf{x}_s \\ x_b \end{Bmatrix} = \begin{bmatrix} \boldsymbol{\Phi}_s & \boldsymbol{\Psi}_s \\ \mathbf{0} & \mathbf{I} \end{bmatrix} \begin{Bmatrix} \boldsymbol{\xi}_s \\ x_b \end{Bmatrix} = \boldsymbol{\Phi} \boldsymbol{\xi} \tag{5}$$

Substituting this into the motion equation of the overall structure and multiplying both sides by $\boldsymbol{\Phi}^{\mathrm{T}}$, we get

$$\boldsymbol{\Phi}^{\mathrm{T}} \mathbf{M} \boldsymbol{\Phi} \ddot{\boldsymbol{\xi}} + \boldsymbol{\Phi}^{\mathrm{T}} \mathbf{C} \boldsymbol{\Phi} \dot{\boldsymbol{\xi}} + \boldsymbol{\Phi}^{\mathrm{T}} \mathbf{K} \boldsymbol{\Phi} \boldsymbol{\xi} = -\boldsymbol{\Phi}^{\mathrm{T}} \mathbf{M} \mathbf{r} \ddot{x}_{\mathrm{g}} - \boldsymbol{\Phi}^{\mathrm{T}} \mathbf{F}_{\mathrm{nl}} \tag{6}$$

which we can simplify as follows:

$$\mathbf{M}^* \ddot{\boldsymbol{\xi}} + \mathbf{C}^* \dot{\boldsymbol{\xi}} + \mathbf{K}^* \boldsymbol{\xi} = -\boldsymbol{\Phi}^{\mathrm{T}} \mathbf{M} \mathbf{r} \ddot{x}_{\mathrm{g}} - \boldsymbol{\Phi}^{\mathrm{T}} \mathbf{F}_{\mathrm{nl}}$$

DOI: 10.1002/stc

$$\boldsymbol{\Phi}^{\mathrm{T}}\mathbf{F}_{\mathrm{nl}} = \begin{bmatrix} \boldsymbol{\Phi}_s^{\mathrm{T}} & \mathbf{0} \\ \boldsymbol{\Psi}_s^{\mathrm{T}} & \mathbf{I} \end{bmatrix} \begin{Bmatrix} \mathbf{0} \\ f_{\mathrm{nl}} \end{Bmatrix} = \begin{Bmatrix} \mathbf{0} \\ f_{\mathrm{nl}} \end{Bmatrix} = \mathbf{F}_{\mathrm{nl}}$$

$$\mathbf{M}^* = \boldsymbol{\Phi}^{\mathrm{T}}\mathbf{M}\Phi = \begin{bmatrix} \boldsymbol{\Phi}_s^{\mathrm{T}} & \mathbf{0} \\ \boldsymbol{\Psi}_s^{\mathrm{T}} & \mathbf{I} \end{bmatrix} \begin{bmatrix} \mathbf{M}_s & 0 \\ 0 & m_b \end{bmatrix} \begin{bmatrix} \boldsymbol{\Phi}_s & \boldsymbol{\Psi}_s \\ \mathbf{0} & \mathbf{I} \end{bmatrix} = \begin{bmatrix} \mathbf{I} & \boldsymbol{\Phi}_s^{\mathrm{T}}\mathbf{M}\mathbf{r}_s \\ \mathbf{M}\mathbf{r}_s^{\mathrm{T}}\boldsymbol{\Phi}_s & \mathrm{tr}(\mathbf{M}) \end{bmatrix}$$

$$\mathbf{K}^* = \boldsymbol{\Phi}^{\mathrm{T}}\mathbf{K}\Phi = \begin{bmatrix} \boldsymbol{\Phi}_s^{\mathrm{T}} & \mathbf{0} \\ \boldsymbol{\Psi}_s^{\mathrm{T}} & \mathbf{I} \end{bmatrix} \begin{bmatrix} \mathbf{K}_s & \mathbf{K}_{sb} \\ \mathbf{K}_{bs} & k_2 + k_b \end{bmatrix} \begin{bmatrix} \boldsymbol{\Phi}_s & \boldsymbol{\Psi}_s \\ \mathbf{0} & \mathbf{I} \end{bmatrix} = \begin{bmatrix} \boldsymbol{\Phi}_s^{\mathrm{T}}\mathbf{K}_s\boldsymbol{\Phi}_s & \mathbf{0} \\ \mathbf{0} & k_b \end{bmatrix} = \begin{bmatrix} \boldsymbol{\omega}^2 & \mathbf{0} \\ \mathbf{0} & k_b \end{bmatrix}$$

$$\mathbf{C}^* = \boldsymbol{\Phi}^{\mathrm{T}}\mathbf{C}\Phi = \begin{bmatrix} \boldsymbol{\Phi}_s^{\mathrm{T}} & \mathbf{0} \\ \boldsymbol{\Psi}_s^{\mathrm{T}} & \mathbf{I} \end{bmatrix} \begin{bmatrix} \mathbf{C}_s & \mathbf{C}_{sb} \\ \mathbf{C}_{bs} & c_2 + c_b \end{bmatrix} \begin{bmatrix} \boldsymbol{\Phi}_s & \boldsymbol{\Psi}_s \\ \mathbf{0} & \mathbf{I} \end{bmatrix} = \begin{bmatrix} \boldsymbol{\Phi}_s^{\mathrm{T}}\mathbf{C}_s\boldsymbol{\Phi}_s & \mathbf{0} \\ \mathbf{0} & c_b \end{bmatrix} = \begin{bmatrix} \alpha\boldsymbol{\omega}^2 & \mathbf{0} \\ \mathbf{0} & c_b \end{bmatrix}$$

where

$$\mathbf{K}_{bs} = \begin{bmatrix} 0 & \cdots & 0 & -k_2 \end{bmatrix} = \mathbf{K}_{bs}^{\mathrm{T}}$$

and

$$\boldsymbol{\Psi}_s^{\mathrm{T}}\mathbf{K}_s + \mathbf{K}_{bs} = 0$$

The final form of the motion equation in the hybrid coordinates is

$$\begin{bmatrix} \mathbf{I} & \boldsymbol{\Phi}_s^{\mathrm{T}}\mathbf{M}\mathbf{r}_s \\ \mathbf{M}\mathbf{r}_s^{\mathrm{T}}\boldsymbol{\Phi}_s & tr(\mathbf{M}) \end{bmatrix} \ddot{\boldsymbol{\xi}} + \begin{bmatrix} \alpha\boldsymbol{\omega}^2 & \mathbf{0} \\ \mathbf{0} & c_b \end{bmatrix} \dot{\boldsymbol{\xi}} + \begin{bmatrix} \boldsymbol{\omega}^2 & \mathbf{0} \\ \mathbf{0} & k_b \end{bmatrix} \boldsymbol{\xi} = -\boldsymbol{\Phi}^{\mathrm{T}}\mathbf{M}\mathbf{r}\ddot{x}_{\mathrm{g}} - \mathbf{F}_{\mathrm{nl}} \tag{7}$$

The new coordinate system could reduce the number of physical parameters significantly. Another advantage of this form is that the complete modal information of the superstructure is not required. The participation factors of higher modes are relatively low for base-isolated buildings. We assume here that only the first n orders of the superstructure are known.

When we consider only first n modes as expressed in the form

$$\mathbf{x}_s = \bar{\boldsymbol{\Phi}}_s\bar{\boldsymbol{\xi}}_s + \boldsymbol{\Psi}_s x_b$$

$$\mathbf{x} = \begin{Bmatrix} \mathbf{x}_s \\ x_b \end{Bmatrix} = \begin{bmatrix} \bar{\boldsymbol{\Phi}}_s & \boldsymbol{\Psi}_s \\ \mathbf{0} & \mathbf{I} \end{bmatrix} \begin{Bmatrix} \bar{\boldsymbol{\xi}}_s \\ x_b \end{Bmatrix} = \bar{\boldsymbol{\Phi}}\bar{\boldsymbol{\xi}}$$

where $\bar{\boldsymbol{\xi}}_s$ is the first n modal coordinates, and $\bar{\boldsymbol{\Phi}}_s$ is the first n columns of $\boldsymbol{\Phi}_s$, in other words, the first n orders of mode shapes.

Following the same procedure, we obtain

$$\begin{bmatrix} \mathbf{I} & \bar{\boldsymbol{\Phi}}_s^{\mathrm{T}}\mathbf{M}\mathbf{r}_s \\ \mathbf{M}\mathbf{r}_s^{\mathrm{T}}\bar{\boldsymbol{\Phi}}_s & tr(\mathbf{M}) \end{bmatrix} \ddot{\bar{\boldsymbol{\xi}}} + \begin{bmatrix} \alpha\bar{\boldsymbol{\omega}}^2 & \mathbf{0} \\ \mathbf{0} & c_b \end{bmatrix} \dot{\bar{\boldsymbol{\xi}}} + \begin{bmatrix} \bar{\boldsymbol{\omega}}^2 & \mathbf{0} \\ \mathbf{0} & k_b \end{bmatrix} \bar{\boldsymbol{\xi}} = -\bar{\boldsymbol{\Phi}}^{\mathrm{T}}\mathbf{M}\mathbf{r}\ddot{x}_{\mathrm{g}} - \bar{\boldsymbol{\Phi}}^{\mathrm{T}}\mathbf{F}_{\mathrm{nl}} \tag{8}$$

Extracting the second row related to the base isolator from Equation (7), we can obtain the following single degree of freedom (DOF) equation of motion for the isolation layer:

$$m_b\ddot{x}_b + c_b\dot{x}_b + k_b x_b = -\mathrm{tr}(\mathbf{M}\mathbf{r}_s)(\ddot{x}_b + \ddot{x}_{\mathrm{g}}) - m_b\ddot{x}_{\mathrm{g}} - \mathbf{M}\mathbf{r}_s^{\mathrm{T}}\boldsymbol{\Phi}_s\ddot{\boldsymbol{\xi}}_s - f_{\mathrm{nl}} \tag{9}$$

Therefore, the identification of the isolation layer has become as simple as possible. The restoring force of the isolation layer can be expressed as follows:

$$F = c_b\dot{x}_b + k_b x_b + f_{\mathrm{nl}} = -\mathrm{tr}(\mathbf{M}\mathbf{r})(\ddot{x}_b + \ddot{x}_{\mathrm{g}}) - \mathbf{M}\mathbf{r}_s^{\mathrm{T}}\boldsymbol{\Phi}_s\ddot{\boldsymbol{\xi}}_s \tag{10}$$

DOI: 10.1002/stc

The restoring force consists of two parts. The first term represents the rigid inertial force of the superstructure, and the second term is the inertial force in modal coordinates.

3. IDENTIFIABILITY OF SUPERSTRUCTURE

The superstructure is to be identified before the restoring force of the isolation layer can be estimated. Consequently, the identifiability problem of the superstructure should be investigated here.

After the system of interest is decomposed into the superstructure and the isolation layer, these two subsystems comprise a complete closed-loop system (Figure 3). The superstructure is considered the plant, and the isolation layer is considered the regulator. The ground acceleration is the reference signal, which is the persistent excitation of any order, input to the overall system. The isolation layer generates the feedback, which is the relative acceleration of this layer with respect to the ground. The absolute acceleration of the layer (which excites the plant) is the sum of this feedback and the reference signal.

The identifiability condition of the closed-loop system was investigated by Ljung, Soderstrom, and Gustavsson [8–10]. The details of this condition will not be elaborated in this paper because that elaboration needs another notation system. For the sake of simplicity, the necessary condition for identifiability is given here as

$$r \geq (n_{\mathrm{y}} + n_u)/(n_{\mathrm{y}} + n_r) \tag{11}$$

where r is the number of regulators and n_y, n_u, and n_r are, respectively, the numbers of plant outputs, plant inputs, and reference signals. In the case of the ground excitation, n_u equals n_r, the regulator is not replaceable, and $r = 1$. Therefore, no matter what the feedback might be, the necessary condition always holds as long as there is ground motion. In other words, the superstructure under earthquakes is strictly system identifiable if the input and the output of the plant are given.

4. SUBSPACE IDENTIFICATION

The subspace identification formulates and solves a major part of the identification problem on a signal level. The main characteristic of these schemes is the approximation of a subspace defined by the span of the column or row space of matrices determined by the input–output data. The parametric time-invariant model is calculated from these spans by exploiting their special structure, such as the shift-invariance property. Subspace identification methods take advantage of robust numerical techniques such as QR factorization and singular

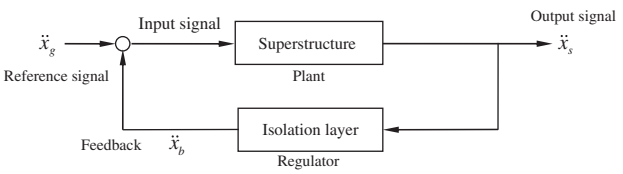

Figure 3. Subsystems in closed-loop scheme.

DOI: 10.1002/stc

value decomposition (SVD). For brevity, only an archetypical procedure is illustrated in this paper.

Given a deterministic–stochastic state-space model with a p-dimensional output y_t and an m-dimensional input u_t,

$$x_{t+1} = Ax_t + Bu_t + w_t$$

$$y_t = Cx_t + Du_t + v_t \tag{12}$$

where w_t and v_t are unmeasurable disturbances, respectively, called process error and measurement error and x is an n-dimensional state-space vector.

From Equation (12) we can formulate the k-step ahead predictor y_{t+k} by expanding x_{t+k}. Then we form the equation

$$Y_r(t) = O_r x_t + S_r U_r(t) + V(t) \tag{13}$$

where

$$Y_r(t) = \begin{bmatrix} y_t \\ y_{t+1} \\ \vdots \\ y_{t+r-1} \end{bmatrix}, \quad U_r(t) = \begin{bmatrix} u_t \\ u_{t+1} \\ \vdots \\ u_{t+r-1} \end{bmatrix}, \quad O_r = \begin{bmatrix} C \\ CA \\ \vdots \\ CA^{r-1} \end{bmatrix}, \quad S_r = \begin{bmatrix} D & 0 & \cdots & 0 \\ CB & D & \cdots & 0 \\ \vdots & \vdots & \ddots & \vdots \\ CA^{r-2}B & CA^{r-3}B & \cdots & D \end{bmatrix}$$

In addition, the kth block component of $V(t)$ is

$$V_k(t) = CA^{k-2}w_t + CA^{k-3}w_{t+1} + \cdots + Cw_{t+k-2} + v_{t+k-1} \tag{14}$$

O_r is the extended observability matrix for the system. To eliminate the term with $U_r(t)$ and make the noise influence from $V(t)$ disappear asymptotically, we introduce

$$\mathbf{Y} = [Y_r(1)\ Y_r(2)\ \cdots\ Y_r(N)]$$

$$\mathbf{X} = [x_1\ x_2\ \cdots\ x_n]$$

$$\mathbf{U} = [U_r(1)\ U_r(2)\ \cdots\ U_r(N)]$$

$$\mathbf{V} = [V(1)\ V(2)\ \cdots\ V(N)]$$

We can rewrite Equation (13) as

$$\mathbf{Y} = O_r\mathbf{X} + S_r\mathbf{U} + \mathbf{V} \tag{15}$$

and form an $N \times N$ matrix orthogonal to the matrix $\mathbf{U}$:

$$\Pi^{\perp}_{\mathbf{U}^{\mathrm{T}}} = \mathbf{I} - \mathbf{U}^{\mathrm{T}}(\mathbf{U}\mathbf{U}^{\mathrm{T}})^{-1}\mathbf{U} \tag{16}$$

Multiplying Equation (15) by $\Pi^{\perp}_{\mathbf{U}^{\mathrm{T}}}$ will eliminate the term with $\mathbf{U}$, yielding

$$\mathbf{Y}\Pi^{\perp}_{\mathbf{U}^{\mathrm{T}}} = O_r\mathbf{X}\Pi^{\perp}_{\mathbf{U}^{\mathrm{T}}} + \mathbf{V}\Pi^{\perp}_{\mathbf{U}^{\mathrm{T}}} \tag{17}$$

By correlating with a suitable matrix Φ [11], the noise term can be removed as well. Thus, we have

$$G = \frac{1}{N}\mathbf{Y}\Pi^{\perp}_{\mathbf{U}^{\mathrm{T}}}\Phi^{\mathrm{T}} \tag{18}$$

DOI: 10.1002/stc

The column space can be reduced by using SVD. If G has rank n, only the first n singular values will be nonzero. Therefore, we have

$$G = \mathrm{USV}^{\mathrm{T}} = [U_1\ U_2]\begin{bmatrix} S_1 & 0 \\ 0 & S_2 \end{bmatrix}\begin{bmatrix} V_1^{\mathrm{T}} \\ V_2^{\mathrm{T}} \end{bmatrix} = U_1 S_1 V_1^{\mathrm{T}} \tag{19}$$

where S_1 is the $n \times n$ upper left part of S.

An estimate of the extended observability matrix may be obtained as $\hat{O}_r = U_1 S_1$. We can finally estimate the system matrices C by using the first block row of O_r and estimate the system matrix A by using the shift property. Once we have C and A, we can estimate the matrices B and D by solving a linear least-squares problem. It is worth noting that the left and right weighting matrices for the oblique projection G determine a wide class of subspace algorithms, such as N4SID [12], MOESP [13], and CVA [14].

5. MODE SHAPE EXPANSION

For economical reason, accelerometers are usually not installed in every story. Therefore, the measured mode shapes consist of a limited number of DOF, typically smaller than the number of DOF in the analytic model. The full-length vector of mode shapes is, however, indispensable in the calculation of the equivalent external force acting on the isolation layer. It is necessary to expand the measured mode shapes for matching the other unmeasured DOFs. The Guyan static expansion [15] is suggested in this paper because of its simplicity.

The Guyan static expansion method is based on the assumption that inertial forces acting on the unmeasured DOFs are negligible with respect to the elastic forces. This assumption is implemented by setting $\mathbf{M} = \mathbf{0}$ in the following modal force equilibrium equation:

$$\left(\begin{bmatrix} \mathbf{K}_{aa} & \mathbf{K}_{ao} \\ \mathbf{K}_{oa} & \mathbf{K}_{oo} \end{bmatrix} - \omega_i^2 \begin{bmatrix} \mathbf{M}_{aa} & \mathbf{M}_{ao} \\ \mathbf{M}_{oa} & \mathbf{M}_{oo} \end{bmatrix}\right)\begin{pmatrix} \phi_{ai} \\ \phi_{ao} \end{pmatrix} = 0 \tag{20}$$

The subscripts a and o, respectively, represent the locations of the measured and the unmeasured DOFs.

This equation leads to an exact analytical relationship between the mode shapes at the measured and unmeasured DOFs:

$$\phi_{ao} = -\mathbf{K}_{oo}^{-1}\mathbf{K}_{oa}\phi_{ai} \tag{21}$$

Usually there is no preknowledge about the stiffness distribution of the superstructure, so we have to use an alternative way to describe it. We assume that the stiffness distribution of a building is proportional to its mass distribution. This assumption is reasonable for buildings with conventional shapes.

6. IDENTIFICATION PROCEDURE

The procedure of the proposed method is illustrated in Figure 4. After the identification process for the superstructure, the number of the unknown parameters to be identified could be reduced

DOI: 10.1002/stc

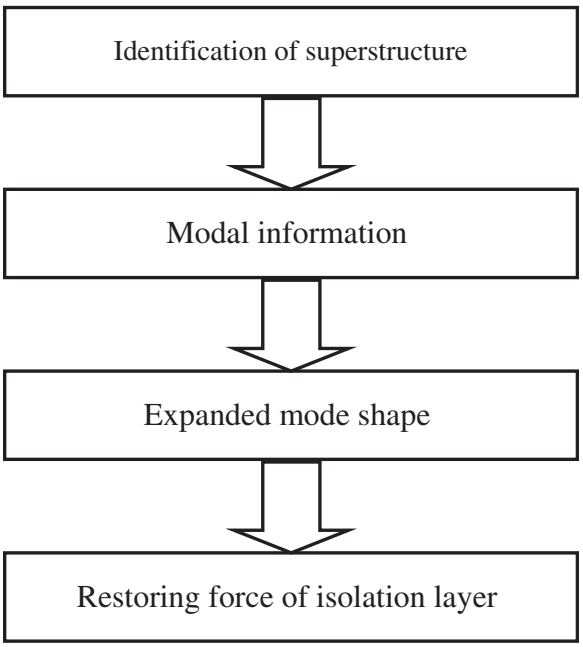

Figure 4. Procedure of the proposed method.

greatly as shown in Equation (9). Only partial modal information is required for the estimation of the restoring force, which makes this method workable when the number of sensors is limited. It is easy to incorporate the nonlinearity in the isolation layer by selecting nonlinear models for the restoring force:

$$F = c_b\dot{x}_b + k_b x_b + f_{\mathrm{nl}} = -\mathrm{tr}(\mathbf{Mr})(\ddot{x}_b + \ddot{x}_{\mathrm{g}}) - \mathbf{Mr}_s^{\mathrm{T}}\boldsymbol{\Phi}_s\ddot{\boldsymbol{\xi}}_s$$

What we want to identify is the total restoring force on the left-hand side of this equation. To do this we first need to specify the mass distribution $\mathbf{Mr}_s$, the expanded mode shape matrix $\boldsymbol{\Phi}_s$, and the acceleration in modal coordinates $\ddot{\boldsymbol{\xi}}_s$ on the right-hand side. Given that the acceleration response at floors is observable, the ground excitation and the acceleration response at the isolation layer and several other floors are known. It is not difficult to retrieve the mode shape information $\boldsymbol{\Phi}_s$ by using subspace identification methods. Only partial modal information is required for the estimation of the restoring force, but the mode shapes need to be expanded at unmeasured DOFs. Then the acceleration in modal coordinates $\ddot{\boldsymbol{\xi}}_s$ can be obtained by the transformation from the physical coordinates. The mass distribution $\mathbf{Mr}_s$ is treated by taking the design value of real buildings, since the mass of buildings hardly changes unless significant rebuilding or retrofitting takes place.

DOI: 10.1002/stc

7. NUMERICAL SIMULATION

A multistory structure supported by a base-isolation layer is considered here. We refer to the part of the structure above the base as the superstructure, and we make the following assumptions:

1. The superstructure is of a shear type, its stiffness and mass may vary from floor to floor, it remains within the elastic range even during an earthquake, and its only nonlinearity is associated with the base-isolation system.
2. The base-isolation layer consists of an elastic spring, a hysteretic damper, and a viscous damper.

According to the experimental observation that the elastomeric bearings and friction-type isolators exhibit little rate dependence and quite stable hysteresis loops [16], a smooth and differential hysteresis model is adopted for the hysteretic dampers in the dynamic simulation. A widely accepted one is the Bouc–Wen hysteresis model proposed by Bouc [17] and generalized by Wen [18] and other researchers [19,20] to incorporate the deterioration of hysteretic characteristics. Although it is not in total accordance with the plasticity theory and sometimes it predicts negative dissipated energy [21], it has been widely used in seismic engineering.

The differential equation of the Bouc–Wen model is

$$D_y \dot{z} = A\dot{u} - (\gamma \operatorname{sgn}(z\dot{u}) + \beta)|z|^n \dot{u} \tag{22}$$

and the hysteretic force of the isolation layer is given by

$$F_h = F_y z$$

The terms D_y and F_y are, respectively, the yield displacement and force of the hysteretic damper; z is a dimensionless parameter; A, β, and γ are parameters that describe the shape of the hysteresis loop; and u and $\dot{u}$ are, respectively, the displacement and velocity of the isolation layer. The smoothness of transition from elasticity to plasticity is determined by n, and when $n \to \infty$ the hysteresis model is reduced to a bilinear case.

A seven-story base-isolated building is considered and the mass and stiffness matrices of the superstructure are shown in Figure 5. The damping matrix is assumed to be proportional to the stiffness matrix and the first order of the damping ratio is 1%. The modal information of the superstructure is listed in Table I. The accelerometers are installed in the basement, on the first story, on the fourth story, and on the roof. The restoring force of the isolation layer is given by

$$F = k_b x_b + c_b \dot{x}_b + F_h$$

The parameters related to the isolation layer are listed in Table II.

The earthquake that happened on 23 July 2005 in the Chiba prefecture, Japan, is selected as the ground input. The ground acceleration was observed at the Hiyoshi Campus of Keio University and was recorded by the Raiosya monitoring system [22]. The maximum acceleration in this record is 70.13 cm/s^2 and the sampling rate is 100 Hz (Figure 6).

The simulation was conducted using Simulink MATLAB®. The acceleration response of the superstructure is illustrated in Figure 7 and the restoring force is plotted against displacement in Figure 8.

Two cases are under consideration: one with the acceleration response contaminated by 1% white noise and the other with the acceleration response contaminated by 10% white noise. Taking the acceleration at the first story as the ground input to the superstructure and the

DOI: 10.1002/stc

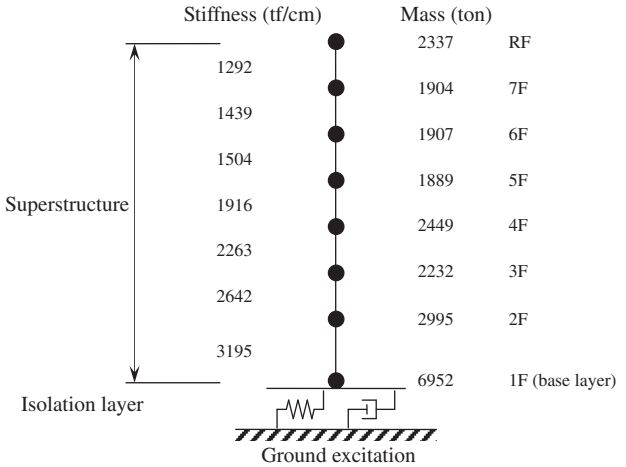

Figure 5. Simulation model of a seven-story base-isolated building.

Table I. Modal information of superstructure.

	Frequency (Hz)	Damping ratio (%)
First	1.09	1.00
Second	2.82	2.59
Third	4.61	4.22
Fourth	6.06	5.55
Fifth	7.36	6.74

Table II. Parameter values.

k_b	475 000 (kN/m)
c_b	6000 (kNs/m)
α	0.0029
β	0.6
γ	0.4
n	1
D_y	1.5 mm
F_y	655.4 (kN)

accelerations at the fourth story and roof as the responses, the mode shapes of the superstructure were identified by the subspace identification method (N4SID) using the toolbox in Matlab. After the first two mode shapes at measured DOFs were extracted (Table III), they were expanded to the unmeasured DOFs by using Equation (21) as shown in Figure 9. In this calculation, the stiffness distribution was assumed to be proportional to the mass distribution.

DOI: 10.1002/stc

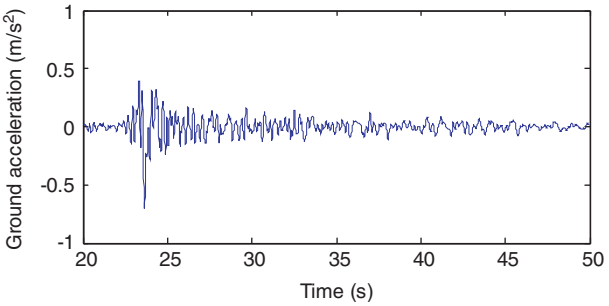

Figure 6. Ground acceleration observed at Hiyoshi.

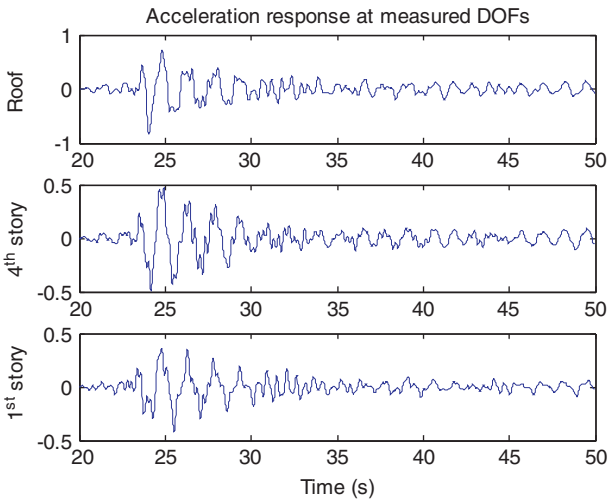

Figure 7. Acceleration response of the superstructure.

The acceleration in modal coordinates $\ddot{\boldsymbol{\xi}}_s$ corresponds to the physical acceleration obtained by coordinate transformation:

$$\ddot{\boldsymbol{\xi}}_s = \boldsymbol{\Phi}_s^{-1}\ddot{\mathbf{x}}^{\mathrm{r}} \tag{23}$$

$\boldsymbol{\Phi}_s^{-1}$ is the pseudo-inverse matrix of the expanded mode shape matrix of $\boldsymbol{\Phi}_s$. The evaluated results and analytical values are plotted in Figures 10 and 11.

All the unknown parameters in Equation (10) needed for estimating the restoring force of the isolation layer were determined assuming the mass to be the same as that in the simulation model. Figure 12 illustrates the difference between the estimated restoring force and the analytical one. Although they are consistent at a rather high level, the estimated force–displacement is distorted a lot (Figure 13). These cases with different noise levels show that noise degrades the identification results, the modal information, and the modal acceleration but has little effect on the estimated restoring force. The reason is that the dominant part of the

DOI: 10.1002/stc

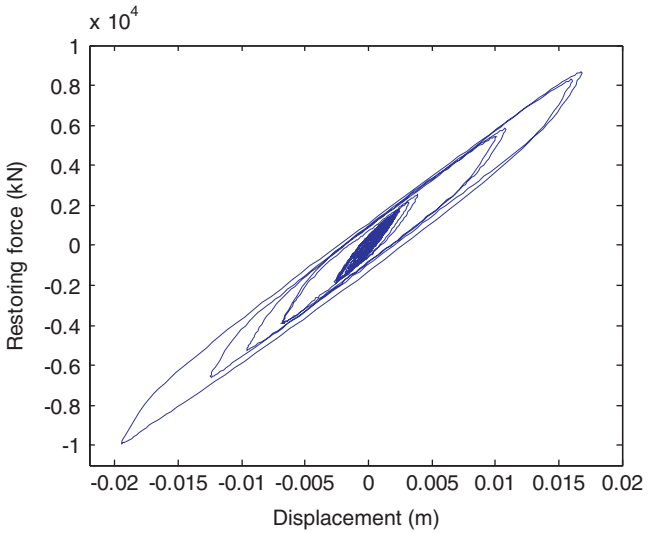

Figure 8. Restoring force of the isolation layer vs displacement.

Table III. Identified mode shapes of superstructure.

	1% noise		10% noise	
	Roof	Fourth story	Roof	Fourth story
First	1	0.4419	1	0.4385
Second	1	−1.0053	1	−1.0281

restoring force comes from the inertia force of the superstructure, and the part coming from modal inertia forces does not count as much.

7.1. Effect of mode selection

The effect of mode selection was examined for three different choices: the first mode, the first two modes, and the first three modes. As illustrated in Figure 14, the first two modes can generate acceptable results. In most cases, the response of the structure is dominated by the low-order vibration modes with high participation factors.

7.2. Effect of mass estimation

The effect of the mass estimation was evaluated by investigating two kinds of mass variation. First, the mass estimation was scaled to its simulation value, in this case, by 90%, and the first two modes were selected for the restoring force estimation. As illustrated in Figure 15, the estimated value retains the shape but is scaled by the same degree. This is due to the reason that the rigid inertial force, which dominates the restoring force, is proportional to the total.

DOI: 10.1002/stc

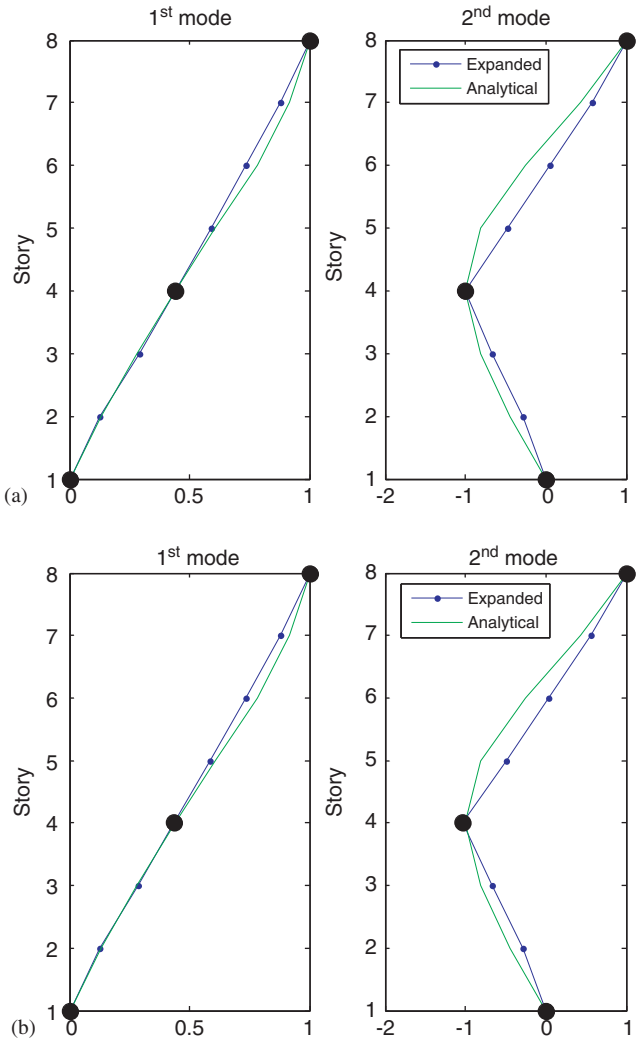

Figure 9. Expanded and analytic mode shapes: (a) 1% noise and (b) 10% noise.

The second kind of mass variation was that the mass is normally distributed around the simulation value with a certain standard deviation (in this case, 20% of the simulation value). As shown in Figure 16, in this case too the estimated value fits the analytical value very well. From these two examples, it is concluded that the estimation of the restoring force is insensitive to the mass distribution but will be scaled by the estimated total mass.

8. APPLICATION TO AN ACTUAL BASE-ISOLATED BUILDING

The proposed method was applied to a building named Raiosya at Keio University in Japan. It is a seven-story base-isolated building 30.95 m high. The structure of the superstructure has a

DOI: 10.1002/stc

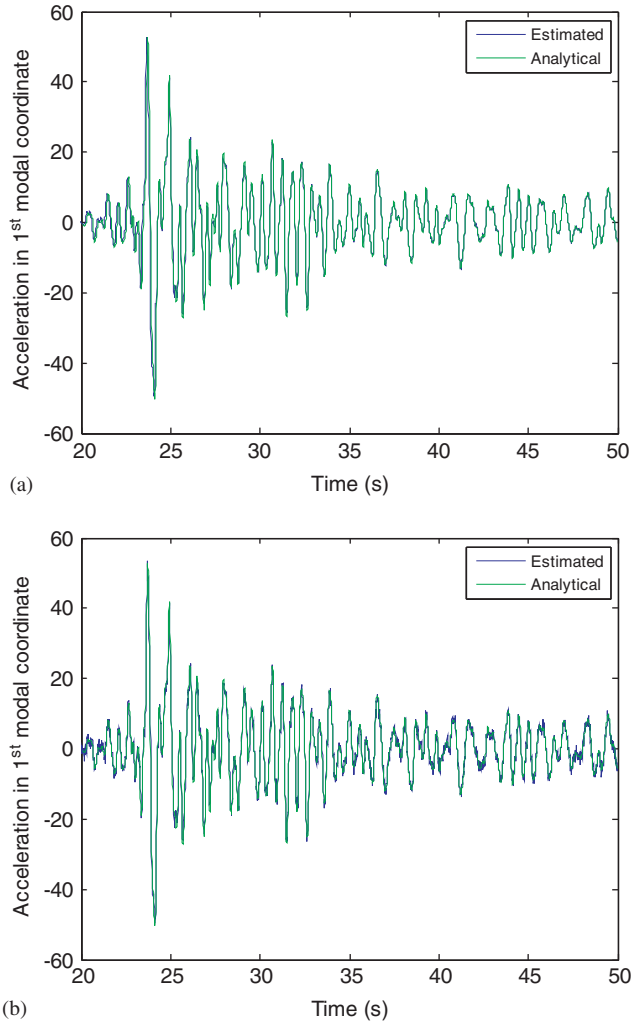

Figure 10. Acceleration in the first modal coordinate $\ddot{\xi}_{1s}$: (a) 1% noise (fitting rate = 92.1%) and (b) 10% noise (fitting rate = 88.6%).

steel frame and the supporting columns are concrete-filled tubes. The base-isolation layer is equipped with three kinds of devices: 55 high-damping rubber bearings 750–900 mm in diameter, 6 oil dampers in each direction, and 9 elastic sliding bearings. As illustrated in Figure 17, the monitoring system installed in this building has 16 accelerometers at 7 locations and 3 displacement sensors at 2 locations. The sampling frequency of these sensors is 100 Hz. The measurements are stored in the monitoring server and can be accessed and downloaded via the Internet.

The earthquake that happened on 23 July 2005 in the Chiba prefecture, Japan, was used for analysis. The movement in the x-plane was considered for the analysis. The ground motion is plotted in Figure 6; the acceleration collected by ♯1, ♯2, ♯4; and ♯5 (shown in Figure 17) in the

DOI: 10.1002/stc

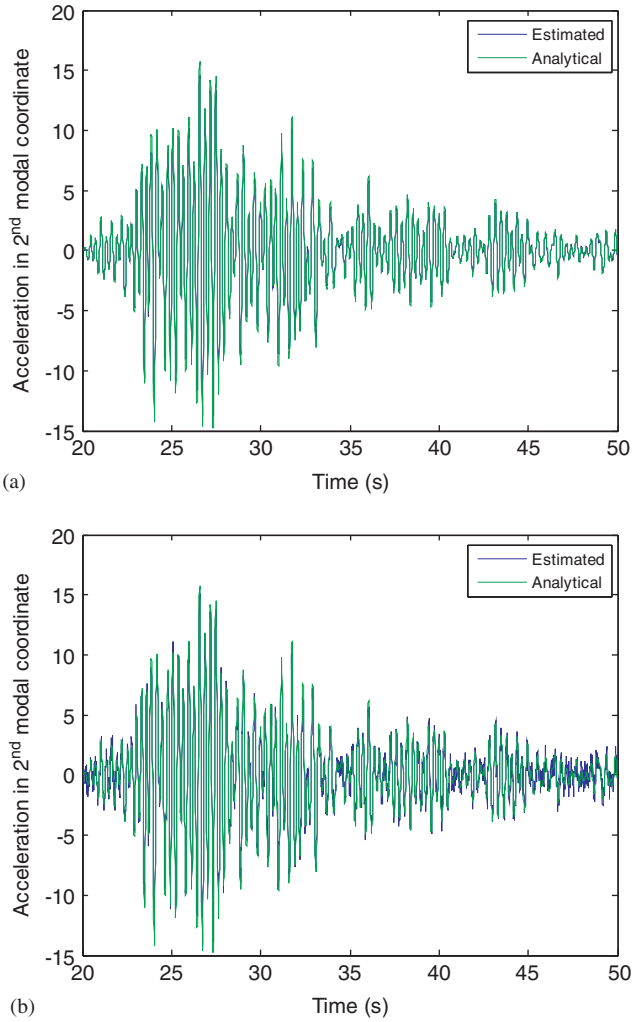

Figure 11. Acceleration in the second modal coordinate $\ddot{\xi}_{2s}$: (a) 1% noise (fitting rate = 90.8%) and (b) 10% noise (fitting rate = 83.3%).

x-direction and the deformation of the isolation layer collected by ♯102 in the x-direction are shown in Figures 18 and 19.

Yoshimoto *et al*. [23] developed an algorithm based on the subspace identification to identify the stiffness of the isolation layer and applied it to Raiosya. In the paper, when the deformation of the layer is small (with the maximum value 0.76 mm in the y-direction), the identification succeeded when applied to the simulation case and the existing building under earthquakes. The method is based on linear models, however, so nonlinear behaviors are not explicitly considered. The nonlinearity in the isolations is the crucial feature accounting for the behavior of the base-isolated system. This nonlinearity will be illustrated by the force–displacement plot showing the

DOI: 10.1002/stc

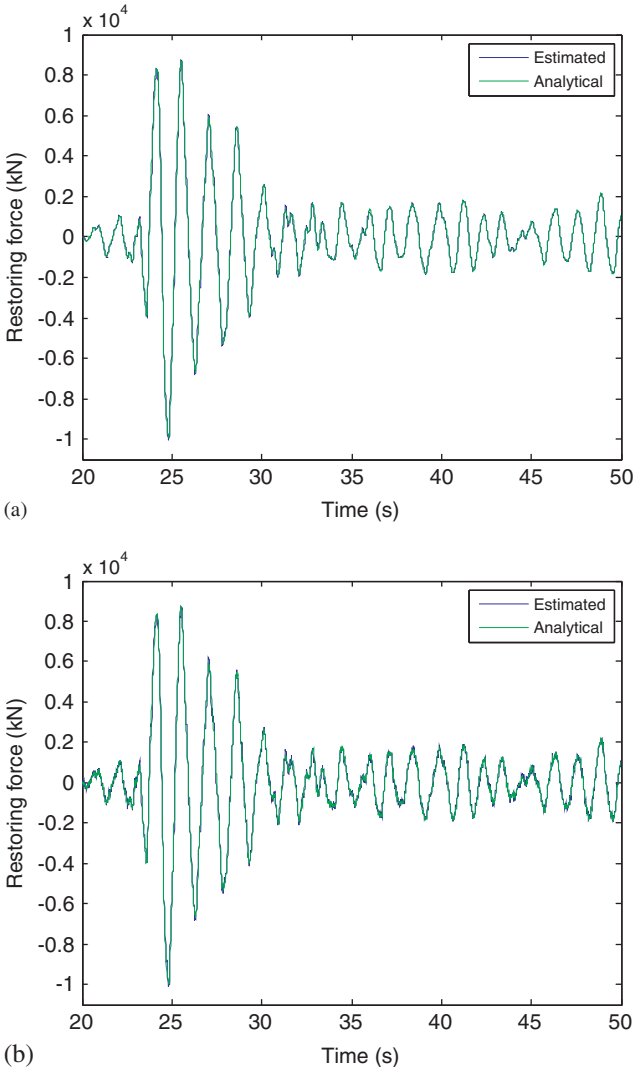

Figure 12. Estimated restoring force of the isolation layer: (a) 1% noise (fitting rate = 94.6%) and (b) 10% noise (fitting rate = 94.1%).

hysteresis, and the amplitude-dependent stiffness and damping coefficient are adopted to relate the nonlinearity with the deformation.

The identification of the superstructure was performed under the assumption that it was a linear lightly damped structure. The mode shapes of the superstructure that were identified by the subspace identification method (N4SID) when the acceleration at the first story was taken as the excitation, and the accelerations at fourth story and roof were taken as the responses listed in Table IV along with other modal information. We then expand the first two

DOI: 10.1002/stc

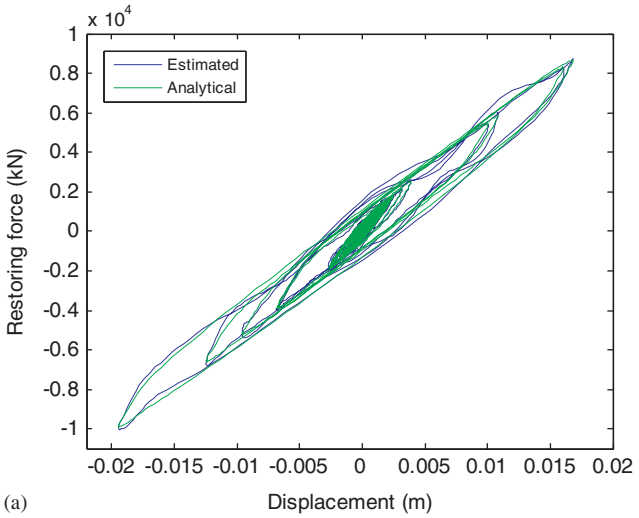

Figure 13. Estimated restoring force vs displacement.

modes (Figure 20) and use the expanded mode shapes to estimate the restoring force. The accelerations in modal coordinates were calculated by transformation (Figure 21).

Assuming the estimated mass to be the simulation value, we were able to estimate the restoring force expressed in Equation (10). Figure 22 shows the estimated result, and Figure 23 shows the force–displacement plot.

Figure 23 indicates that the isolation layer has strong hysteresis due to its large deformation. However, it is difficult to extract intrinsic state information of the isolation layer from the force–displacement plot. As stated by Stewart *et al.* [3] and Tobita [4], the performance of the base-isolated system depends on the vibration intensity. Therefore, it is feasible to represent

DOI: 10.1002/stc

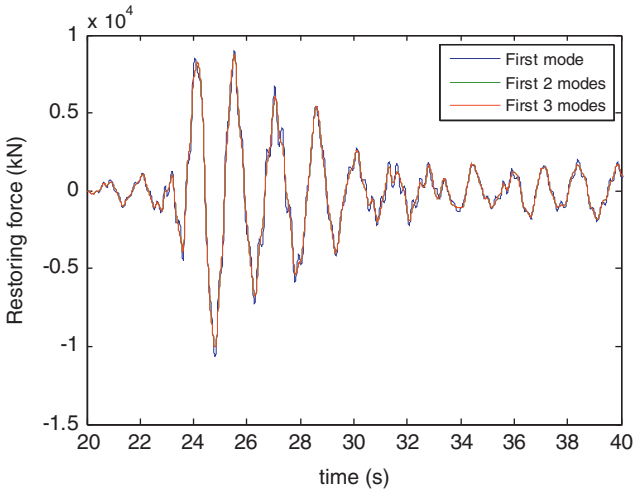

Figure 14. Effect of mode selection on estimation (1% noise).

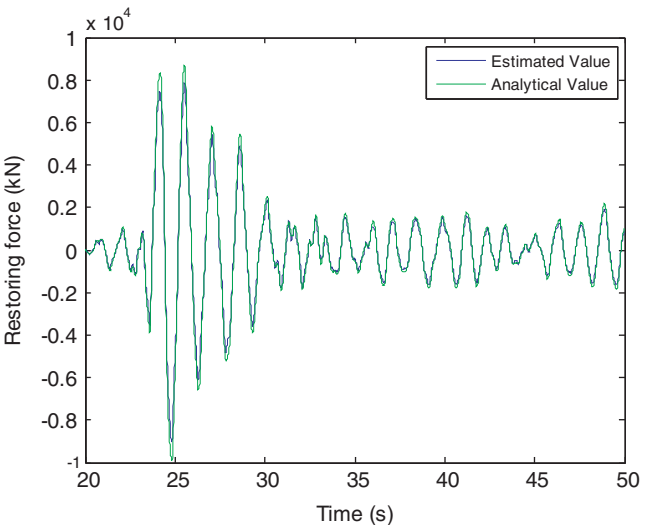

Figure 15. Effect of mass estimation (1% noise).

the state condition of the isolation layer by the equivalent stiffness and damping coefficient, which are evaluated with respect to the deformation of the isolation layer.

If we assume that the restoring force consists of the equivalent elastic force and the equivalent viscous force, we can write

$$f(\dot{x}_b, x_b) = k_{\text{eq}} x_b + c_{\text{eq}} \dot{x}_b \tag{24}$$

DOI: 10.1002/stc

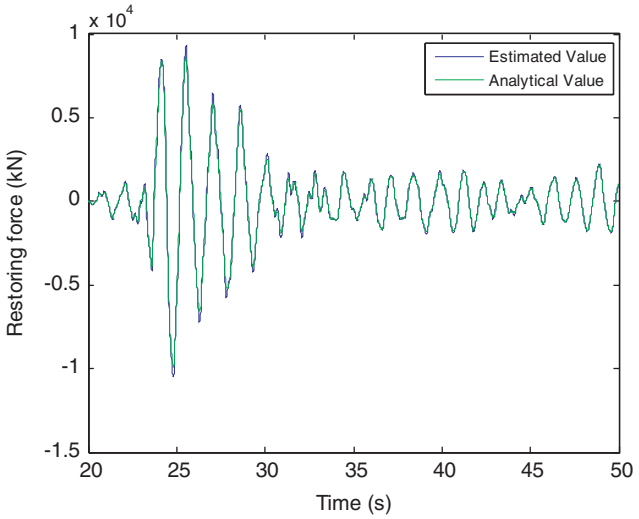

Figure 16. Effect of mass estimation (fitting rate = 93.09%). Mass = [2560.3 1796.5 1637.7 2407.5 2210.9 2351.7 3085.6 7947.9] from the top.

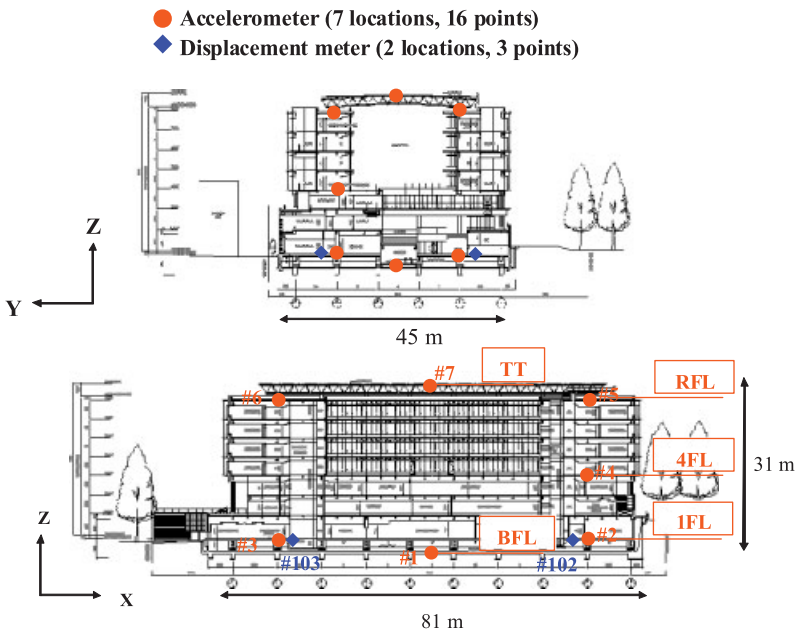

Figure 17. Elevation views showing sensor allocation.

In addition, the restoring force at time t can be estimated by substituting the recorded displacement and velocity into

$$f(t) = [x_b(t)\ \dot{x}_b(t)] \begin{bmatrix} k_{eq} \\ c_{eq} \end{bmatrix} = \mathbf{H}_t \mathbf{P} \tag{25}$$

DOI: 10.1002/stc

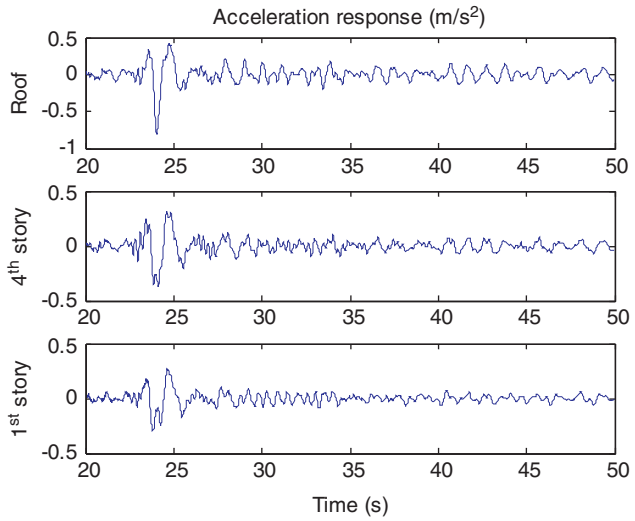

Figure 18. Acceleration response (♯2 ♯4 ♯5 in x direction).

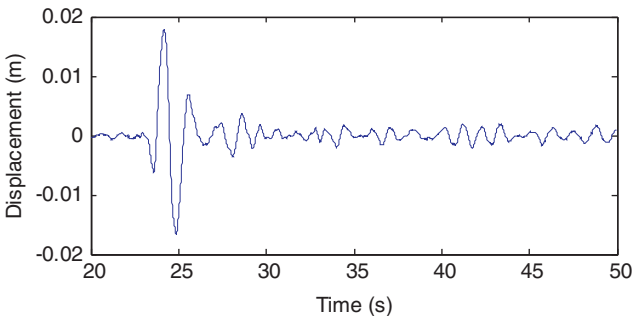

Figure 19. Deformation of the isolation layer (♯102 in the x-direction).

Table IV. Identified modal information of superstructure.

			Mode shape	
	Freq.	Damping	Roof	Fourth story
First	1.0819	0.0347	1	0.3680
Second	3.4720	0.0445	1	−1.4671

The minimum least-squares approximation of the coefficient is given by

$$\mathbf{P} = (\mathbf{H}^{\mathrm{T}}\mathbf{H})^{-1}\mathbf{H}^{\mathrm{T}}\mathbf{f} \tag{26}$$

DOI: 10.1002/stc

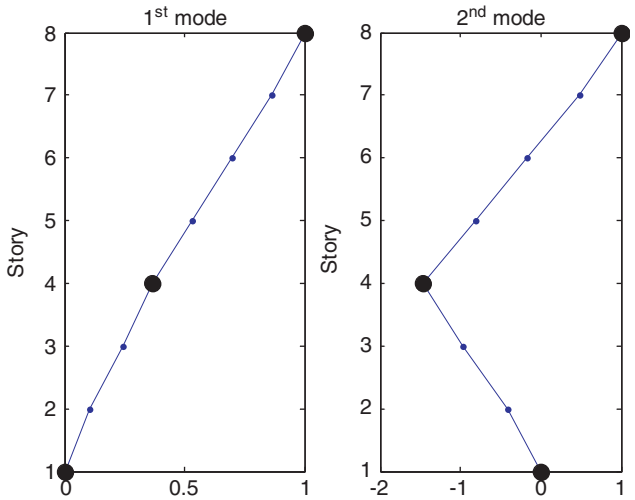

Figure 20. Expanded mode shape.

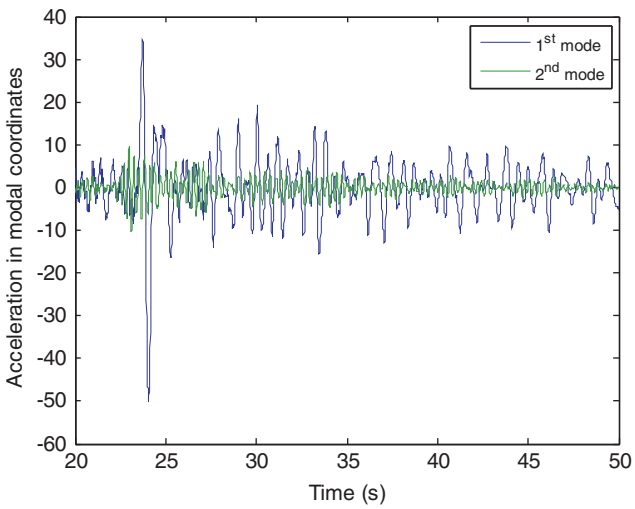

Figure 21. Acceleration in modal coordinates.

The recorded data were sliced into segments, and the equivalent coefficients were estimated within each segment. The average amplitude of the displacement was evaluated by using the following equation:

$$A_{\text{eq}} = \sqrt{2}\text{RMS}(x_b) \tag{27}$$

where RMS is the root mean square function.

The estimated stiffness and damping coefficient in the x-plane are plotted against the displacement amplitude in Figure 24. Both of them decrease with increasing amplitude, as usual, the estimation of the equivalent stiffness is more stable than that of the damping coefficient. The

DOI: 10.1002/stc

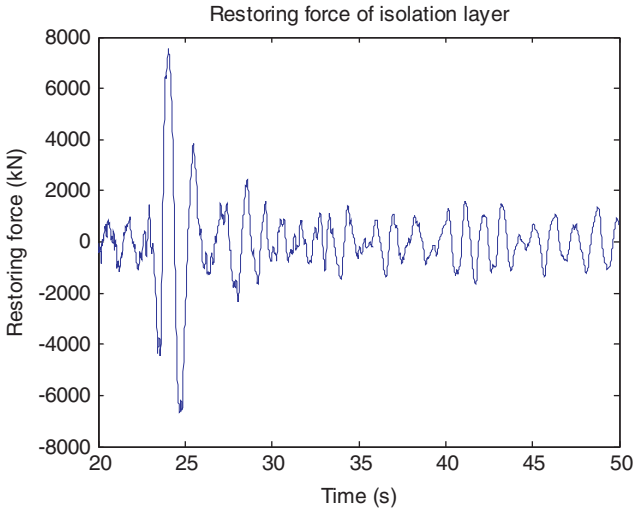

Figure 22. Restoring force of the isolation layer.

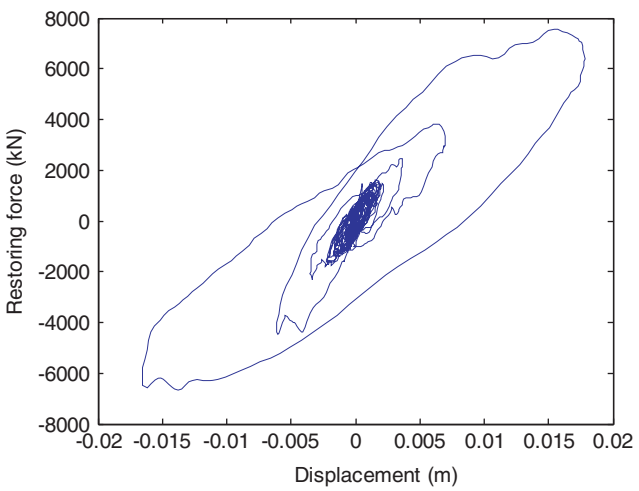

Figure 23. Force–displacement plot.

stiffness is very sensitive in the small amplitude range and might drop 50% at a shear strain of 2.5% (the 100% shear strain is at 0.2-m displacement in the design book for Raiosya). Compared with the small amplitude experiment performed by Abe *et al*. [2], the same decreasing pattern is confirmed.

9. CONCLUSION

This paper represented a new method, based on the CMS, for estimating the restoring force of an isolation layer. The hybrid motion equation involving the modal coordinates and the

DOI: 10.1002/stc

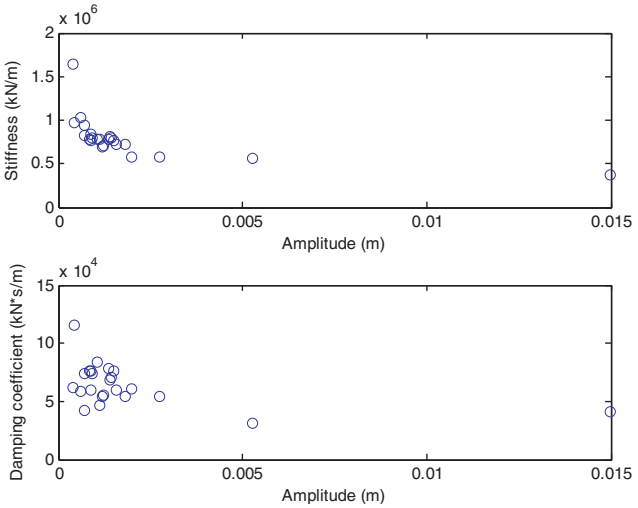

Figure 24. Equivalent stiffness and damping coefficient.

physical coordinates is derived by using a substructuring technique. This method is applicable when the number of sensors is limited because only the mode shape information of the superstructure and the estimated mass estimation are needed for estimating the restoring force. It was shown that the proposed method is not sensitive to the mass distribution and the expanded mode shapes but will be scaled by the total mass. The effectiveness of this method was validated in simulations and in application to an actual base-isolated building. In this paper, the amplitude-dependent equivalent stiffness and damping coefficient are adopted to describe the nonlinearity of the isolation layer. The identified results by our proposed method reconfirm the experimental observation of nonlinearity in the layer made up of isolators.

REFERENCES

1. Doebling S, Farrar C, Prime M, Shevitz D. Damage identification and health monitoring of structural and mechanical systems from changes in their vibration characteristics: a literature review. *LA–13070-MS*, Los Alamos National Lab., NM, 1996.
2. Abe M, Yoshida J, Fujino Y. Multiaxial behaviors of laminated rubber bearings and their modeling. I: experimental study. *Journal of Structural Engineering, American Society of Civil Engineers* 2004; **130**:1119–1132.
3. Stewart J, Conte J, Aiken I. Observed behavior of seismically isolated buildings. *Journal of Structural Engineering* 1999; **125**:955–964.
4. Tobita J. Evaluation of nonstationary damping characteristics of structures under earthquake excitations. *Journal of Wind Engineering & Industrial Aerodynamics* 1996; **59**:283–298.
5. Hurty W. Vibrations of structural systems by component-mode synthesis. *Journal of the Engineering Mechanics Division (ASCE)* 1960; **86**:51–69.
6. Craig R. A review of time–domain and frequency–domain component mode synthesis method. *Combined Experimental/Analytical Modeling of Dynamic Structural Systems*, *Proceedings of the Joint Mechanics Conference*, Albuquerque, NM, June 1985; 1–30.
7. Craig R, Bampton M. Coupling of substructures for dynamic analysis. *AIAA Journal* 1968; **6**:1313–1319.
8. Ljung L, Gustavsson I, Soderstrom T. Identification of linear, multivariable systems operating under linear feedback control. *IEEE Transactions on Automatic Control* 1974; **19**:836–840.

DOI: 10.1002/stc

9. Soderstrom T, Ljung L, Gustavsson I. Identifiability conditions for linear multivariable systems operating under feedback. *IEEE Transactions on Automatic Control* 1976; **21**:837–840.
10. Gustavsson I, Ljung L, Soderstrom T. Identification of processes in closed loop—identification and accuracy aspects. *Automatica* 1977; **13**:59–75.
11. van Overschee P, De Moor B. *Subspace Identification for Linear System, Theory, Implementation, Applications*. Kluwer Academic Publishers: Dordrecht, 1996.
12. van Overschee P, De Moor B. N4SID: numerical algorithms for state space subspace system identification. *Proceedings of the IFAC World Congress*, Sydney, July 1993; 361–364.
13. Verhaegen M. Identification of the deterministic part of MIMO state space models given in innovations form from input–output data. *Automatica* 1994; **30**:61–67.
14. Larimore W. Canonical variate analysis in identification, filtering, and adaptive control. *Proceedings of the 29th IEEE Conference on Decision and Control*, Honolulu, HI, December 1990; 596–604.
15. Guyan R. Reduction of stiffness and mass matrices. *AIAA Journal* 1965; **3**:380.
16. Yoshida J, Abe M, Fujino Y. Constitutive model of high-damping rubber materials. *Journal of Engineering Mechanics, American Society of Civil Engineers* 2004; **130**:129–141.
17. Bouc R. Forced vibration of mechanical systems with hysteresis. *Proceedings of the 4th Conference on Nonlinear Oscillations*, Prague, September 1967.
18. Wen YK. Method for random vibration of hysteretic systems. *Journal of the Engineering Mechanics Division* 1976; **102**:249–263.
19. Baber T, Noori M. Modeling general hysteresis behavior and random vibration application. *Journal of Vibration, Acoustics, Stress, and Reliability in Design, American Society of Mechanical Engineers* 1986; **108**:411–420.
20. Baber TT, Wen YK. Random vibration hysteretic, degrading systems. *Journal of the Engineering Mechanics Division* 1981; **107**:1069–1087.
21. Carli F. Nonlinear response of hysteretic oscillator under evolutionary excitation. *Advances in Engineering Software* 1999; **30**:621–630.
22. Yoshimoto R, Mita A, Okada K, Iwaki H, Shiraishi M. Damage detection of a structural health monitoring system for a 7-story seismic isolated building. *Smart Structures and Materials 2003: Smart Systems and NDE for Civil Infrastructures, Proceedings of SPIE*, vol. 5057, San Diego, 2003; 594–605.
23. Yoshimoto R, Mita A, Okada K. Damage detection of base-isolated buildings using multi-input multi-output subspace identification. *Earthquake Engineering & Structural Dynamics* 2005; **34**:307–324.

DOI: 10.1002/stc